Magnetohydrodynamic-calibrated edge-localized mode model in simulations of International Thermonuclear Experimental Reactor

Thawatchai Onjun
Sirindhorn International Institute of Technology, Klong Luang, Pathumthani 12121, Thailand

Arnold H. Kritz and Glenn Bateman
Physics Department, Lehigh University, 16 Memorial Drive East, Bethlehem, Pennsylvania 18015

Vassili Parail
*European Atomic Energy Community (EURATOM)/United Kingdom Atomic Energy Authority (UKAEA),
Fusion Association, Culham Science Centre, Abingdon, OX14 3DB, United Kingdom*

Self-consistent simulations of the International Thermonuclear Experimental Reactor (ITER) [R. Aymar, P. Barabaschi, and Y. Shimomura, Plasma Phys. Controlled Fusion **44**, 519 (2002)] have been carried out using the JETTO-integrated modeling code in which theory-motivated models are used for the *H*-mode pedestal and for the stability conditions that lead to the edge-localized mode (ELM) crashes. Transport is described by combining the anomalous mixed Bohm/gyro-Bohm model [M. Erba, A. Cherubini, V. V. Parail, and A. Taroni, Plasma Phys. Controlled Fusion **39**, 261 (1997)] with the NCLASS neoclassical transport model [W. A. Houlberg, K. C. Shaing, S. P. Hirshman, and M. C. Zarnstorff, Phys. Plasmas **4**, 3231 (1997)] in the core region, while only neoclassical transport is used in the pedestal region. In the simulations, an ELM crash can be triggered either by a pressure-driven ballooning mode or by a current-driven peeling mode, depending on which instability reaches its stability criterion first. The equilibrium and magnetohydrodynamics (MHD) stability analyses codes, HELENA and MISHKA [A. B. Mikhailovskii, G. T. A. Huysmans, S. E. Sharapov, and W. Kerner, Plasma Phys. Rep. **23**, 713 (1997)], are used to evaluate the edge stability of the plasma just prior to an ELM crash in order to calibrate and confirm the validity of the stability criteria used to trigger ELMs in the JETTO simulations. It is found that the simulation of the ITER baseline case yields a fusion *Q* of 16.6, with the electron and ion temperatures at the top of the pedestal of 4.4 and 4.9 keV, respectively. The high values of the pedestal temperature result from access to the second stability region of the ballooning mode. Simulation sensitivity studies are carried out by varying parameters such as the auxiliary heating power and the width of the pedestal. When the auxiliary heating power is turned off, it is found that significant fusion power is sustained and that access to ballooning mode second stability is maintained. © *2005 American Institute of Physics*. [DOI: 10.1063/1.2007547]

I. INTRODUCTION

High-confinement mode (*H*-mode) discharges in tokamaks provide good energy confinement and have acceptable particle transport rates for impurity control. Because of these properties, *H*-mode is one of the scenarios that will be used in burning plasma experiments such as the International Thermonuclear Experimental Reactor (ITER).[1] However, *H*-mode discharges are often perturbed by quasiperiodic bursts of magnetohydrodynamics (MHD) activity at the edge of the plasma, which are known as edge-localized modes (ELMs). Each ELM crash results in a rapid loss of particles and energy from the edge of the plasma, which can reduce the average global energy content by 10%–20%.[2] Furthermore, these transient bursts of energy and particles into the scrape-off layer produce high-peak heat loads on the divertor plates. On the other hand, the ELMs remove heat and particles, including impurities, from the region near the separatrix. ELMs also play an essential role in the control of the pedestal height in *H*-modes, and it has been shown both in experiments and in simulations that the parameters at the top of the pedestal have a strong influence on the performance of *H*-mode discharges.[3–6] Consequently, the production of fusion power in ITER is expected to depend sensitively on the behavior of ELMs.

In recent ITER studies, simulations have been carried out to predict the performance of ITER using several integrated modeling codes, such as BALDUR,[7] XPTOR,[8] and ASTRA.[9] The BALDUR simulations for ITER were carried out from the center of the plasma to the top of the pedestal without including the effect of ELM crashes.[10] The temperature at the top of the pedestal, T_{ped}, is one of the boundary conditions required in BALDUR *H*-mode simulations. In Ref. 10, T_{ped} was calculated using a simple pedestal temperature model in which the pressure gradient is limited by the first ballooning stability and the pedestal width is based on magnetic shear and flow shear stabilization.[11] A similar treatment for the boundary conditions is used in the ITER simulations with the XPTOR code.[5] The simulations of ITER carried out using the BALDUR code and the XPTOR code do not include the effect of ELMs. Somewhat more advanced simulations of ITER have been carried out using the ASTRA code.[12] In these

simulations, the pedestal is produced by $E \times B$ shear and magnetic shear stabilization, and a simple model of ELMs, based on the pressure-driven ballooning mode, is employed to simulate the effect of ELMs in a time-averaged fashion. However, the ELM model that was used did not include triggering of ELMs resulting from current-driven peeling modes. Simulations carried out using the ASTRA code yielded, for JET and ASDEX-Upgrade ELMy *H*-mode discharges, temperature profiles similar to the experimental profiles, and, for ITER, values of fusion Q in the range of 12–16.

In this paper, self-consistent simulations of the standard *H*-mode ITER scenario are carried out using the JETTO modeling code[13] in which theory-motivated models are used for the *H*-mode pedestal and for the stability conditions that lead to the ELM crashes. Transport is described by combining the anomalous mixed Bohm/gyro-Bohm model[13] with the NCLASS neoclassical transport model.[14] In the pedestal region, which is assumed to extend 6 cm inside the separatrix—thus the top of the pedestal is located approximately at the radius $\rho = 0.95$—in the baseline case, the anomalous transport is completely suppressed and, consequently, the neoclassical transport dominates. The reduction of transport within the pedestal region results in a steep pressure gradient at the edge of the plasma, which, in turn, produces a large bootstrap current density in the pedestal. The steep edge pressure gradient and the large edge bootstrap current can trigger either an unstable pressure-driven ballooning mode or an unstable current-driven peeling mode, resulting in an ELM crash. In the simulations, an ELM crash is triggered by a pressure-driven ballooning mode if, anywhere within the pedestal region, the pressure gradient exceeds the ballooning mode stability limit, or an ELM crash is triggered by a current-driven peeling mode if the edge current density exceeds the critical edge current density of the peeling condition. These stability conditions are included in the JETTO code. The equilibrium and MHD stability analyses codes, HELENA and MISHKA,[15] are then used to evaluate the edge stability of the plasma just before an ELM crash in order to calibrate and confirm the validity of the stability criteria that are used to trigger ELMs in the JETTO simulations. The stability analyses include infinite-*n* ideal ballooning modes, finite-*n* ballooning modes, and low-*n* kink/peeling modes.

H-mode simulations of JET discharges, using the same transport modeling and the combination of pressure-driven ballooning modes and current-driven peeling modes to trigger ELM crashes described above, have been carried out for a number of standard *H*-mode scenarios. The scans include a triangularity scan,[16] a power scan,[17] and a gas-puffing scan.[18] The simulations yielded temperature profiles that were in reasonable agreement with experimental data and resulted in a better understanding of the pedestal and ELMs in *H*-mode plasmas.[19,20]

This paper is organized as follows. The transport code, JETTO, and equilibrium and stability codes, HELENA and MISHKA, are briefly described in Sec. II. ITER simulation results and the associated stability analyses are presented in Sec. III. The dependence of the value of fusion Q on the assumed width of the pedestal and on the heating power is examined in Sec. IV and the test of self-sustained heating is carried out in Sec. V. The conclusions are contained in Sec. VI.

II. MODELING CODES

In this paper, simulations of an ITER scenario are carried out using the predictive JETTO code and MHD stability analyses are carried out using the HELENA and MISHKA codes. These codes are described in this section.

A. The JETTO code

The $1\frac{1}{2}$D JETTO transport code is used to evolve the plasma current, temperatures, and density profiles throughout the plasma, including both the core and pedestal regions. The core transport is calculated using the mixed Bohm/gyro-Bohm model[13] together with the NCLASS neoclassical model.[14] For the pedestal region, two assumptions are applied in this paper. One assumption is that of the pedestal width which is fixed equal to 6 cm. (This assumption is relaxed in Sec. IV in order to examine the dependence of the simulation results on pedestal width.) The second assumption is that the anomalous turbulent transport is completely suppressed in the region between the top of the pedestal and the separatrix, resulting in the establishment of a steep gradient region. In the pedestal region prior to an ELM crash, transport is computed by taking all the diagonal elements of the transport matrix within the pedestal equal to the ion neoclassical thermal conductivity, calculated at the top of the pedestal using NCLASS.[14] The use of constant ion neoclassical diffusion in the pedestal region is based on the consideration that since the pedestal width is usually of the order of the ion orbit width (or banana width), there is limited variation in the neoclassical transport across the barrier. The boundary conditions for the electron and ion temperatures and for the ion density are imposed at the separatrix in the simulations. The electron and ion temperatures at the separatrix are taken to be 20 eV, and the deuterium and tritium densities at the separatrix are assumed to be 3.5×10^{19} m^{-3}. It is found that the values used for the electron and ion temperatures at the separatrix influence the time evolution of the ELMs, but do not affect the overall confinement,[16] particularly since strong gas puffing was not used.[18]

In the JETTO simulations, the reduced transport within the pedestal region results in the development of a steep pressure gradient, which causes an increase in the bootstrap current within the pedestal. The increase of edge pressure gradient, and the associated increase in the edge current density, leads to a destabilization of either a pressure-driven ballooning mode[21,22] or a current-driven peeling mode.[23–25] The resulting MHD instability triggers an ELM crash, which causes a loss of plasma energy and particles to the wall.

The criterion used in the JETTO simulation for an ELM crash triggered by a pressure-driven ballooning mode is that the normalized pressure gradient, α, anywhere within the pedestal exceeds the critical value of the normalized pressure gradient, α_c:

TABLE I. Notation used in this paper.

Symbol	Units	Description
a	m	Plasma minor radius (half-width)
r	m	Flux surface minor radius (half-width)
R	m	Major radius to geometric center of each flux surface
κ		Plasma elongation
δ		Plasma triangularity
B_T	Tesla	Vacuum toroidal magnetic field at R
I_p	MA	Plasma current
A_H	amu	Hydrogenic isotope mass
$Z_{\rm eff}$		Effective charge
n_l	10^{19} particles/m^3	Line average density
$W_{\rm ped}$	MJ	Stored energy in pedestal region
$T_{e,\rm ped}$	keV	Electron temperature at the top of the pedestal
$n_{e,\rm ped}$	10^{19} particles/m^3	Electron density at the top of the pedestal
$\bar{n}_{20}$	10^{20} particles/m^3	Line average electron density
$P_{\rm NBI}$	MW	NBI Heating power
p	Pa	Plasma pressure
q		safety factor
ρ		Normalized radius
μ_0	H m^{-1}	Permeability of free space
α		Normalized pressure gradient
α_c		Normalized critical pressure gradient of ballooning mode

$$\alpha \equiv -\frac{2\mu_0 q^2}{B_T^2}\frac{R}{a}\frac{\partial p}{\partial \rho} > \alpha_c, \qquad (1)$$

where α_c is a prescribed number that is calibrated employing the stability analyses carried out using the HELENA and MISHKA codes. Note that the notation and units used in this paper are described in Table I. The criterion for an ELM crash triggered by a current-driven peeling mode is that the edge current density exceeds a critical current density. This critical current density model is based on an analytical expression developed in Ref. 23. For axisymmetric toroidal geometry, the current-driven peeling instability condition is

$$\sqrt{1-4D_M} + C_{\rm vac} < 1 + \frac{1}{\pi q'}\oint \frac{\mu_0 j_\parallel B_T}{R^2 B_p^3}dl, \qquad (2)$$

where D_M is the Mercier coefficient, which is proportional to the pressure gradient; $C_{\rm vac}$ is a parameter related to the vacuum energy, which is taken to be 0.2 for the baseline simulations in this study; q' is the derivative of the safety factor with respect to the poloidal flux; $j_\parallel$ is the current density parallel to the magnetic field $\mathbf{B}$; R is the major radius; B_p is the poloidal magnetic field; and dl is the poloidal arclength element for the integral around a flux surface. According to Ref. 23, all parameters in Eq. (2) are evaluated at the plasma edge. However, in this work, an average peeling criterion over a width of 1 cm inside the separatrix is used to prevent unnecessary ELM crashes due to minor plasma profile fluctuations. Note that the edge plasma profiles before an ELM crash are then evaluated using stability analysis codes, HELENA and MISHKA, in order to validate the ELM criteria in these simulations. The stability analyses using HELENA and MISHKA are carried out from the normalized radius $\rho=0.9$ to the edge of the plasma ($\rho=1.0$).

When the condition for an ELM crash is satisfied in the JETTO simulation, either by the pressure-driven ballooning mode criterion [Eq. (1)] or by the current-driven peeling mode criterion [Eq. (2)], an ELM crash is produced as follows: The diagonal transport coefficients for electron and ion thermal transport within the pedestal are temporarily increased to 300 times the ion neoclassical diffusivity at the top of the pedestal, while the particle transport coefficients in the pedestal are increased to 100 times the ion neoclassical diffusivity at the top of the pedestal. Since the theoretical modeling of the transport multiplication factors is not fully developed, the choice for the transport multiplication factors was taken from the simulations of the JET experiments, which reproduce in the simulations the values of the JET experimental ELM frequency and the plasma energy content.[16–18] The increased levels of transport are maintained for a time interval $\tau_{\rm ELM}=0.5$ ms, which is of the order of a typical type-I ELM crash duration in JET. The large increase of the transport within the pedestal leads to a rapid loss of particles and energy. A wide range of H-mode simulations have been carried out using this ELM crash treatment, and it has been demonstrated that these simulations reproduce the plasma profiles in the corresponding JET discharges.[16–18]

B. MHD stability codes

In this paper, MHD stability analyses are carried out using the HELENA and MISHKA codes.[15] The HELENA code is employed to compute the stability of infinite-n ideal ballooning modes and, based on the plasma profiles and equilibrium

TABLE II. The basic parameters of ITER design.

| Physical quantity	ITER
Major radius R (m)	6.2
Minor radius a (m)	2.0
Plasma current I_p (MA)	15.0
Toroidal magnetic field B_T (Tesla)	5.3
Elongation at the separatrix κ_x	1.85
Triangularity at the separatrix δ_x	0.48
Average ion mass [amu]	2.5
$\langle n_{e,20} \rangle$	1.0
$n_{G,20}$	1.2
$\langle n_e \rangle / n_G$	0.8
P_{NBI} (MW)	33.0
P_{RF} (MW)	7.0
Z_{eff}	1.4

FIG. 1. Profiles for ion and electron temperatures (top) and electron density (bottom) are shown as a function of normalized minor radius at a time just prior to an ELM crash. In the upper panel, the solid line shows the ion temperature and the dashed line shows the electron temperature.

information generated by the JETTO code, produces an equilibrium with the higher resolution that is needed for the MISHKA code analyses. MISHKA is then applied to evaluate the stability criteria for finite-n ballooning and low-n kink (peeling) modes. In this study, the stability analysis carried out with the MISKHA code is for modes with toroidal mode number $n=1$ to $n=14$. Note that the version of the MISHKA code used in this paper is based on the ideal MHD model.

III. SIMULATION RESULTS AND DISCUSSION

A. Baseline simulation

The ITER simulation is carried out for the baseline parameters shown in Table II using the JETTO code. The core transport is calculated using the mixed Bohm/gyro-Bohm transport model[13] for the anomalous transport and the NCLASS model[14] for the neoclassical transport. The effect of sawtooth oscillations, which periodically reduce the central plasma profiles, is also included. For simplicity, it is assumed that the mixing radius of each sawtooth oscillation extends from the plasma center up to $q=\sqrt{2}$ radius and that each sawtooth crash occurs every 10.0 s. The pedestal width Δ is assumed to be equal to 6 cm in the baseline simulations. Thus, the top of the pedestal is located at a normalized radius of approximately $\rho=0.95$. There are a number of pedestal width scalings proposed in the literature, such as $\Delta \propto \rho_i s^2$,[11,16,26] $\Delta \propto R\sqrt{\beta_\theta}$,[11,27] and $\Delta \propto \sqrt{\rho_i Rq}$,[11] where ρ_i is the ion gyro-radius, s is the magnetic shear, β_θ is the normalized poloidal pressure, R is the major radius, and q is the safety factor. For $\Delta \propto \rho_i s^2$, the ITER pedestal width is approximately 5.0 cm; for $\Delta \propto R\sqrt{\beta_\theta}$, the pedestal width is approximately 6.0 cm; and for $\Delta \propto \sqrt{\rho_i Rq}$, the width is approximately 4.7 cm. In Sec. IV, the value of the pedestal width is varied to study the sensitivity of the predicted fusion power as a function of this parameter. It is assumed that the effective charge Z_{eff} is 1.4, which results from only carbon impurity, and that the input power is equal to 40 MW. The sensitivity of the performance of ITER to the level of input power is examined in Sec. IV. The radiation profile is taken to be the same as in the JET discharge 52009. The ITER
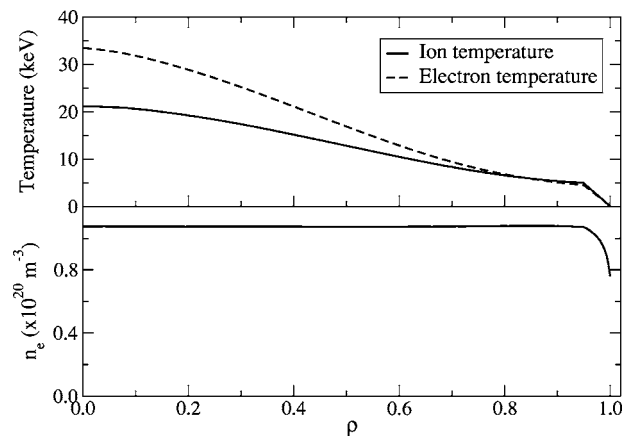
simulations are carried out for discharges with a 50:50 mixing of deuterium and tritium.

Figure 1 shows the ion and electron temperatures and electron density profiles at a time just prior to an ELM crash. It can be seen that the central electron temperature is about 33.3 keV, while the central ion temperature is about 21.0 keV. The central electron temperature is higher than the central ion temperature due to the alpha heating power produced by the fusion reactions. The central ion and electron temperatures obtained in the ITER simulation carried out using the JETTO code are higher than those obtained in the corresponding simulation carried out using the BALDUR code.[10] The differences in the values of the central temperatures in the JETTO and BALDUR simulations are due, in part, to differences in the values of the temperatures at the top of the pedestal. In the JETTO simulations, the ion and electron pedestal temperatures prior to an ELM crash are approximately 4.9 and 4.4 keV, respectively, while in the BALDUR simulations the corresponding pedestal temperatures are 2.7 keV.[10] The temperature profiles in the type-I ELMy H-mode plasma depend on the temperatures at the top of the pedestal.[3,4] The pedestal temperature model used in the BALDUR code was derived based on the assumption that the pedestal pressure gradient is limited by the first-ballooning-mode instability limit. In this study, however, it is found that the ITER plasma obtains access to the ballooning-mode second stability region, which results in a higher edge pressure gradient and, consequently, a higher pedestal temperature. Another difference between the JETTO simulations described in this paper and those carried out previously with the BALDUR code is that the mixed Bohm/gyro-Bohm core transport model is used in the JETTO simulations, while the Multimode (MMM95) core transport model was used in the BALDUR simulations in Ref. 10. In addition to the ITER temperature profiles, the simulated density profile is shown in Fig. 1 at a time just prior to an ELM crash. It can be seen than the density profile is relatively flat, which is similar to the density profile obtained in the ITER BALDUR simulations in Ref. 10. Although the neoclassical transport model includes a par-
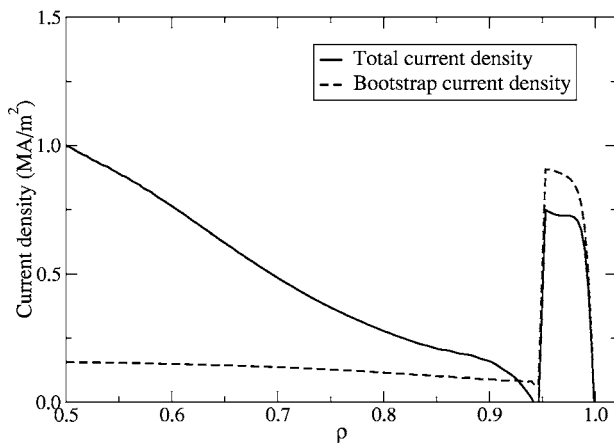
FIG. 2. Profiles for plasma current density and bootstrap current density are shown for the outer half of the plasma. These profiles are taken at the time just prior to an ELM crash. The solid line indicates the total plasma current density and the dashed line is the bootstrap current density.
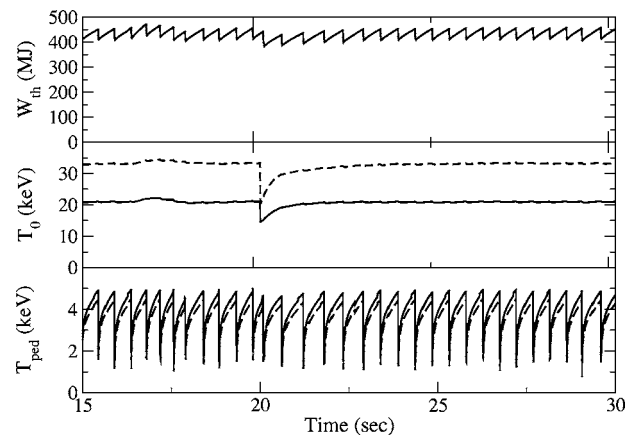

FIG. 3. The plasma stored energy (top panel), the central temperatures (middle panel), and the pedestal temperatures (bottom panel) are plotted as a function of time for the baseline ITER simulation. The electron temperatures are plotted as dashed lines while the ion temperatures are plotted as solid lines.

ticle pinch (the Ware pinch), the anomalous mixed Bohm/gyro-Bohm transport model does not.

In the simulation shown in Fig. 1, the anomalous transport is calculated using the mixed Bohm/gyro-Bohm transport model. The mixed Bohm/gyro-Bohm transport model has two components: the Bohm term (which is proportional to the gyroradius) and the gyro-Bohm term (which is proportional to the gyroradius squared). The details of this transport model can be found in Ref. 13. It is found in this simulation that the gyro-Bohm term dominates over much of the plasma. This result is opposite to the previous H-mode study using the mixed Bohm/gyro-Bohm carried out by Hannum *et al.*[28] In that work, simulations were carried for 22 JET and DIII-D H-mode discharges obtained from the International Profiles Database.[29] In those simulations, the transport was dominated by the nonlocal Bohm term, in which the transport throughout the plasma is proportional to a finite difference approximation to the edge temperature gradient. Hence, in those simulations, the core transport depended somewhat sensitively on the value of the pedestal temperature, T_{ped}. In the ITER simulations reported here, the transport across most of the plasma is dominated by the gyro-Bohm term, which, in the mixed Bohm/gyro-Bohm model, depends only on local plasma parameters and is not very sensitive to the temperature gradient. As a result, the core transport model used in this paper is only moderately sensitive to the value of T_{ped}. This will lead to an explanation given in Sec. IV for the insensitivity of the fusion Q as a function of the value of T_{ped}.

Figure 2 shows the plasma current density and bootstrap current density for outer half of the plasma (from $\rho=0.5$ to $\rho=1.0$) at a time just prior to an ELM crash. It can been seen that the current density is peaked at the edge of the plasma, which is a consequence of the bootstrap current density. Because of the large edge current density, the magnetic shear decreases to a relatively low value within the pedestal, which can lead to a possible access to the second stability region of ballooning modes. It is interesting to note that the bootstrap current density within the pedestal is larger than the total

plasma current density within the pedestal. This effect is caused by the back EMF, which prevents the fast growth of the plasma current density within the pedestal, while the bootstrap current can grow rapidly as a consequence of the pressure gradient. This effect has been observed and explained in a previous study using the JETTO code.[17]

The effects of ELM crashes are included in the JETTO simulations presented in this paper. An ELM crash can be triggered either by a pressure-driven ballooning mode or by a current-driven peeling mode. The effects of ELM crashes on the plasma stored energy and temperature are shown in Fig. 3. It is found that approximately 10% of stored energy at the time just before an ELM crash (45 MJ) is lost during each ELM crash. An ELM crash results in a decrease of plasma pressure in the region between $\rho=0.8$ and $\rho=1.0$. Note that the approximately 30% drop in central temperature at 20 s in the middle panel of Fig. 3 is the result of a sawtooth crash, not an ELM crash.

There are two types of auxiliary heating used in the ITER simulation. The total amount of neutral beam injection (NBI) heating power, P_{NBI}, is 33 MW. The NBI heating profiles are calculated using the Pencil module (http://adas.phys.strath.ac.uk) with a 1-Mev negative ion beam. The NBI heating profiles for electrons and ions are shown in Fig. 4. Another source of auxiliary heating is the RF heating, P_{RF}. The total amount of RF heating power is 7 MW. The RF heating profiles are taken from the JET high-performance discharge 52009, although it is recognized that the physics of RF heating might be different in the ITER plasma. Note that Ohmic heating is small compared to other types of heating. The alpha heating power, P_{α}, is also shown in Fig. 4. It can be seen that the alpha heating power, which is about 133 MW power, dominates over other types of heating and the alpha heating power is peaked at the center of the plasma. With this amount of alpha heating power, the fusion Q, defined as $Q \equiv 5P_{\alpha}/(P_{NBI}+P_{RF})$, is about 16.6.
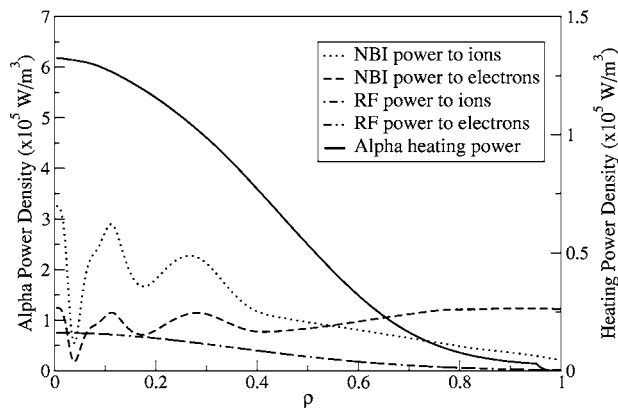
FIG. 4. The alpha heating power density profile is plotted with a solid line using the axis on the left, while the NBI heating power density to the ions (dotted line) and electrons (dashed line) and the RF heating power density (chained lines) are plotted using the axis on the right. In this simulation, 40 MW of auxiliary heating is used (33 MW of NBI heating power and 7 MW of RF heating power). The alpha heating power from the fusion reaction is about 133 MW.

B. Stability analysis

In order to check the validity of the analytical ballooning stability criterion used in the JETTO code, the results of the JETTO simulations are linked with the HELENA and MISHKA MHD stability analysis codes. The HELENA code takes as input the self-consistent equilibrium produced by the JETTO code, that is, the pressure gradient and the current density profiles, together with the corresponding magnetic configuration, at a time just before an ELM crash occurs. The HELENA code then refines the equilibrium in order to provide the resolution required for the stability analysis. The refined equilibrium is used in the HELENA code to generate a ballooning stability s-α diagram and is used in the MISHKA code to evaluate the stability criteria for finite-n ballooning and low-n kink/peeling modes. In this study, the stability analysis is carried out in MISHKA for toroidal mode numbers in the range of $n=1-14$. Note that the version of the MISHKA code employed in this paper is based on the ideal MHD model without dissipation or flow shear.

A stability analysis is carried out using the HELENA and MISHKA codes to evaluate the edge stability at the time just before an ELM crash. Figure 5 shows the stability s-α diagram for the baseline ITER simulation. In the figure, the stability s-α diagram is plotted for four flux surfaces within the pedestal at $\rho=0.95$, 0.96, 0.97, and 0.98. The circle symbol in each panel represents the location of the operational point for the pressure gradient and magnetic shear at that flux surface. The region of instability associated with the infinite-n ideal ballooning modes is indicated with crosses, while the numbers indicate the most unstable mode of finite-n ballooning and low-n kink/peeling modes at each location on the s-α plane.

It can be seen in Fig. 5 that there is a wide access to the second stability region of ballooning modes. Note that the operational point at each flux surface, indicated by the circle symbol, is located at a value of alpha, the normalized pressure gradient, which is significantly higher than the peak value of alpha allowed by the first stability limit. The edge
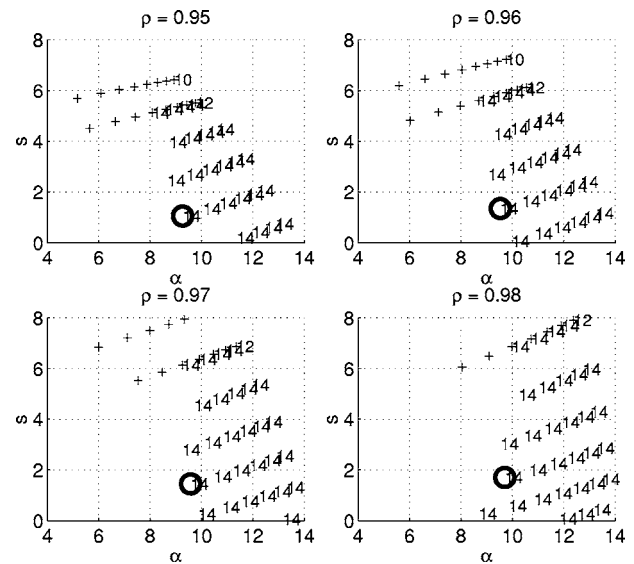

FIG. 5. Stability results obtained using the HELENA and MISHKA stability codes are plotted on an s-α stability diagram at four surfaces within the pedestal ($\rho > 0.94$) for the baseline ITER simulation. The region of instability associated with the infinite-n ideal ballooning modes is indicated with crosses. The numbers indicate the most unstable finite-n ballooning and low-n kink/peeling modes at each location on the s-α plane. Higher mode numbers ($n \geqslant 10$) correspond to finite-n ballooning modes. The region without numbers or crosses is the region where all modes are stable.

pressure gradient appears to be limited by an $n=14$ toroidal mode. The access to the second stability is probably a result of the strong shaping of the ITER plasma, particularly the fact that the ITER plasma is designed to have a triangularity of 0.48 at the separatrix. In the present-day experiments, evidence of access to second stability in high-triangularity discharges has been observed in a number of tokamaks, for example, DIII-D,[30–32] JET,[16] JT-60U,[32–34] and Alcator C-Mod.[35]

IV. SENSITIVITY STUDIES

A. Variation of heating power

In Ref. 1, the scaling of the heating power required for the transition from L-mode to H-mode, P_{L-H}, is expressed as

$$P_{L-H}(MW) = 2.84 A_H^{-1} B_T^{0.82} \bar{n}_{20}^{-0.58} R^{1.00} a^{0.81}, \qquad (3)$$

where $\bar{n}_{20}$ is the line average density in units of 10^{20} particles/m^3. Based on Eq. (3), the L-H transition power required for ITER is about 48 MW. In the simulations shown in Fig. 1, it is found that with the levels of 33-MW NBI heating power, P_{NBI}, and 7-MW RF heating power, P_{RF}, the total heating power, including the alpha heating power ($P_\alpha + P_{NBI} + P_{RF}$), is about 173 MW, which is well above the heating power needed to make the transition from L-mode to H-mode ($P_{L \to H}$).

The simulations of ITER are carried with the auxiliary heating power varied. The level of the total auxiliary heating power is varied from 20 to 50 MW by increasing the NBI heating power from 13 to 43 MW and keeping the RF heating fixed at 7 MW. It is found that with a total auxiliary heating power of 20 MW (13 MW of NBI and 7 MW of
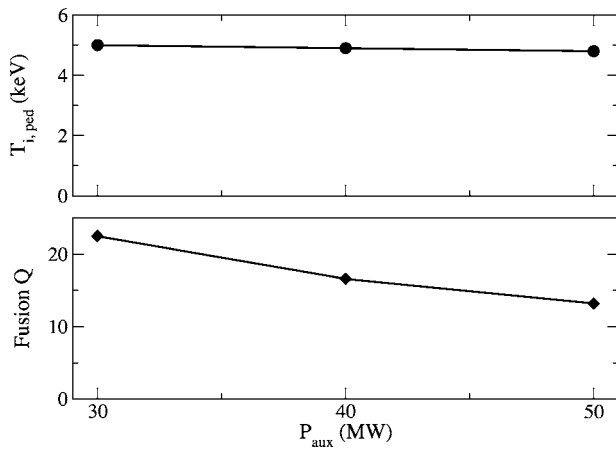
FIG. 6. The pedestal temperature (top panel) and fusion Q (bottom panel) are shown as functions of the auxiliary heating power.
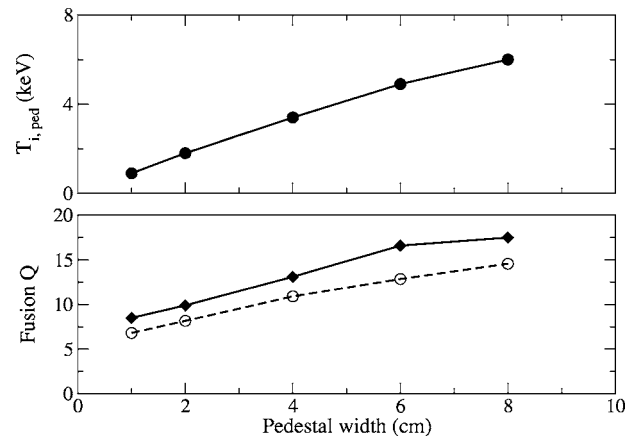

FIG. 7. The pedestal temperature and fusion Q are plotted as functions of the pedestal width for JETTO simulations using the mixed-Bohm/gyro-Bohm transport model (solid line) and corresponding BALDUR simulations using the Multimode transport model (dashed line in bottom panel).

RF), the ion temperature at the top of the pedestal is about several hundreds of electron volts. This plasma is likely to be in L-mode, rather than H-mode. The results of simulations with a total auxiliary heating power of 30–50 MW are shown in Fig. 6, where the average pedestal temperature and average fusion Q at a time just before an ELM crash are indicated for three values of the auxiliary heating power ($P_{NBI}+P_{RF}$). The Ohmic heating power is omitted since it is small compared to the auxiliary heating power. It can be seen in Fig. 6 that as the auxiliary heating power increases, the pedestal temperature remains almost constant. The constancy of pedestal temperature with heating power is not surprising since each sequence of ELM crashes in these simulations is initially triggered by a ballooning mode and the ballooning mode criterion in Eq. (1) is independent of heating power. Consequently, the pressure gradient before an ELM crash is the same in simulations with different levels of auxiliary heating power. With a fixed pedestal width, this results in a pedestal with a relatively constant pedestal temperature prior to each ELM crash. It is found in these simulations that the central ion temperature is nearly constant at 21 keV.

B. Variation of pedestal width

If the core transport model is stiff, the core profiles and fusion performance Q depend on the values of temperature and pressure at the top of the pedestal. One parameter that controls the height of the pedestal is the width of the pedestal. The scaling of the pedestal width is still unclear. Previous experimental studies of pedestal scalings have found a range of results for the pedestal width in various tokamaks.[11] Some studies have found a scaling consistent with a pedestal width that is linearly proportional to the gyroradius.[36–39] Earlier JET results indicated a weaker scaling for the inferred pedestal width—with the pedestal width Δ scaling as $\Delta \propto R(\rho_\theta/R)^\nu$, where ν is in the range of $1/2-2/3$,[40] R is the plasma major radius, and ρ_θ is the poloidal ion gyroradius. Some early studies from DIII-D indicated that it was hard to distinguish between $\Delta/R \propto (\rho_\theta/R)^{2/3}$ and $\Delta/R \propto \beta_\theta^{1/2}$ (where β_θ is the plasma pressure normalized by the poloidal magnetic pressure), but later experiments with a pumped divertor

were able to reduce the correlation between density and plasma current, and they supported a pedestal width scaling $\Delta/R \propto \beta_\theta^{1/2}$.[27] It is found that the pedestal width scalings in Ref. 11 yield a pedestal width in ITER in the range of 4.7–6.0 cm (5.0 cm with $\Delta \propto \rho_i s^2$, 6.0 cm with $\Delta \propto R\sqrt{\beta_\theta}$, and 4.7 cm with $\Delta \propto \sqrt{\rho_i Rq}$).

Simulations of ITER are carried out using the mixed Bohm/gyro-Bohm anomalous transport model in the JETTO code in which the value of the pedestal width is varied from 1 to 8 cm. In this scan, the NBI heating power and RF heating are held fixed at 33 and 7 MW, respectively. In Fig. 7, results from these simulations are shown with solid lines for the average pedestal temperature and the fusion Q at the time just before an ELM crash, plotted as functions of the pedestal width. It can be seen that the pedestal temperature and the fusion Q both increase significantly as the pedestal width increases. The dashed line in the bottom panel in Fig. 7 shows the fusion Q that is predicted using the Multimode anomalous transport model in the BALDUR code.[10] In the BALDUR simulations, the temperature at the top of the pedestal is used as the boundary condition at the edge of the plasma, and ELM crashes are not simulated. It is assumed that the temperature at the top of the pedestal, which is shown in the top panel of Fig. 7, is almost independent of the anomalous transport model that is used in the plasma core, since the time evolution of T_{ped} in the model used here depends only on the width of the pedestal, the neoclassical transport at the top of the pedestal, and the MHD instability condition that triggers each ELM crash.

In these simulations, it is also found that the energy loss due to an ELM crash depends on the width of the pedestal. In simulations with a pedestal width of 2, 4, 6, and 8 cm, the energy loss during each ELM crash is about 21, 39, 45, and 64 MJ, respectively, which corresponds to 7%, 10%, 11%, and 13% of the total plasma energy just before the ELM crash.

V. TEST OF SELF-SUSTAINING HEATING

It is useful to study the issue of self-sustained heating (ignition) in ITER. Does the ITER discharge continue to produce a large amount of fusion power after the auxiliary heat-
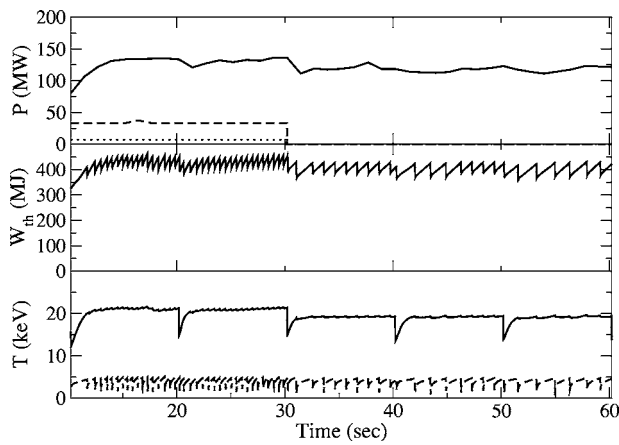
FIG. 8. In the top panel, the time history of the NBI heating (dashed line), RF heating (dotted line), and alpha power heating (solid line) are shown. The auxiliary heating was turned off at 30 s. In the middle panel, the time history of the stored energy is shown. In the bottom panel, the time history of the central ion temperature (solid line) and the pedestal ion temperature (dashed line) are shown. The central ion temperature decreases slightly after the auxiliary heating is turned off, while the pedestal ion temperature remains almost constant.

FIG. 10. Stability results obtained using the HELENA and MISHKA stability codes are plotted on an s-α stability diagram with flux surfaces ranging from $\rho = 0.95$ (top of the pedestal) to $\rho = 0.98$ for the ITER simulation after the auxiliary heating power is turned off. The details of the stability diagram can be found in the caption of Fig. 5.

ing power is turned off? The JETTO code is used to carry out simulations with the 40-MW auxiliary heating power turned off at 30 s. In this simulation, the pedestal width is held fixed at 6 cm. The time history of NBI, RF and alpha power (top panel), thermal energy (middle panel), and central and pedestal temperatures (bottom panel) are shown in Fig. 8. It can be seen that after the auxiliary heating is turned off, the central ion temperature decreases only slightly, which results in a small reduction in the alpha power. On the other hand, the pedestal ion temperature remains almost constant, while the ELM frequency decreases by more than a factor of 2. The fusion reactions are sustained at a level of about 100 MW of alpha power.

Figure 9 shows the ion and electron temperature profiles at a time just prior to an ELM crash before and after the auxiliary power is turned off. It can be seen that the central ion and electron temperatures at a time after the auxiliary

heating is turned off are only slightly lower than that before the auxiliary heating is turned off. The electron and ion pedestal temperatures remain almost the same.

A stability analysis is carried out using the HELENA and MISHKA codes to evaluate the edge stability at a time just before an ELM crash for the ITER simulation after the auxiliary heating power is turned off. In Fig. 10, the stability s-α diagram is plotted for the $\rho = 0.95$, 0.96, 0.97, and 0.98 flux surfaces within the pedestal. It can be seen that the plasma still has access to the second stability region of ballooning modes, which is similar to the result before turning off the auxiliary heating power. The edge pressure gradient appears to be limited by an $n = 14$ toroidal mode.

VI. CONCLUSION

Self-consistent simulations of ITER have been carried out using the JETTO-integrated modeling code in which theory-motivated models are used for the H-mode pedestal and for the stability conditions that lead to the ELM crashes. In these simulations, ELM crashes appear as a sequence of ELM crashes, in which the first ELM crash is triggered by a pressure-driven ballooning mode and the rest are triggered by a current-driven peeling mode. It is found that the baseline simulation of the ITER design yields a fusion Q of 16.6, with the pedestal height about 5 keV. The high value of the pedestal temperature results from access to the second stability of ballooning mode. The fusion Q decreases as the auxiliary heating power increases. Also, the fusion Q decreases as the width of the pedestal decreases. It is found in the simulations that the ITER plasma can sustain alpha power production and access to the second stability of ballooning modes after the auxiliary heating power is shut down.
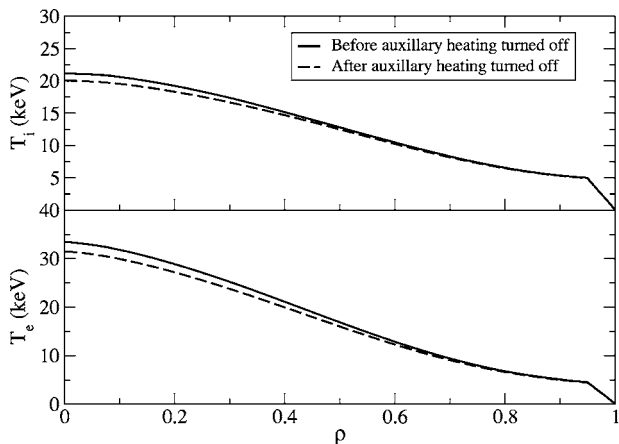

FIG. 9. Profiles for the ion and electron temperatures are shown at the time just prior to an ELM crash. The solid line is at a time when the auxiliary heating is on, while the dashed line is at a time after the auxiliary heating is turned off.
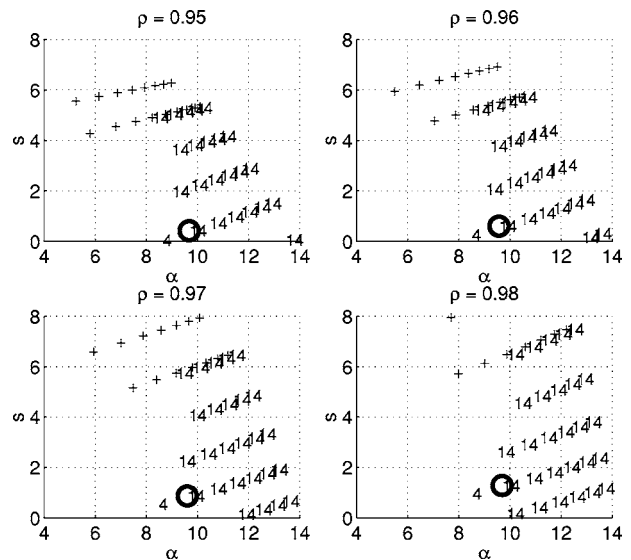
[1] R. Aymar, P. Barabaschi, and Y. Shimomura, Plasma Phys. Controlled Fusion **44**, 519 (2002).

[2] J. W. Connor, Plasma Phys. Controlled Fusion **40**, 191 (1998).

[3] W. Suttrop, M. Kaufmann, H. J. de Blank *et al.*, Plasma Phys. Controlled Fusion **39**, 2051 (1997).

[4] M. Greenwald, R. L. Boivin, F. Bombarda *et al.*, Nucl. Fusion **37**, 793 (1997).

[5] J. Kinsey, T. Onjun, G. Bateman, A. H. Kritz, A. Pankin, G. M. Staebler, and R. E. Waltz, Nucl. Fusion **43**, 1845 (2003).

[6] V. Mukhovatov, Y. Shimomura, A. Polevoi *et al.*, Nucl. Fusion **43**, 942 (2003).

[7] C. E. Singer, D. E. Post, D. R. Mikkelsen *et al.*, Comput. Phys. Commun. **49**, 275 (1988).

[8] J. E. Kinsey, G. M. Staebler, and R. E. Waltz, Phys. Plasmas **9**, 1676 (2002).

[9] G. Janeschitz, G. W. Pacher, O. Zolotukhin, G. Pereverzev, H. D. Pacher, Y. Igitkhanov, G. Strohmeyer, and M. Sugihara, Plasma Phys. Controlled Fusion **44**, A459 (2002).

[10] G. Bateman, T. Onjun, and A. H. Kritz, Plasma Phys. Controlled Fusion **45**, 1939 (2003).

[11] T. Onjun, G. Bateman, A. H. Kritz, and G. Hammett, Phys. Plasmas **9**, 5018 (2002).

[12] G. W. Pacher, H. D. Pacher, A. S. Kukushkin, G. Janeschitz, and G. Pereversev, Nucl. Fusion **43**, 188 (2003).

[13] M. Erba, A. Cherubini, V. V. Parail, and A. Taroni, Plasma Phys. Controlled Fusion **39**, 261 (1997).

[14] W. A. Houlberg, K. C. Shaing, S. P. Hirshman, and M. C. Zarnstorff, Phys. Plasmas **4**, 3231 (1997).

[15] A. B. Mikhailovskii, G. T. A. Huysmans, S. E. Sharapov, and W. Kerner, Plasma Phys. Rep. **23**, 844 (1997).

[16] T. Onjun, A. H. Kritz, G. Bateman, V. Parail, J. Lönnroth, and G. Huysmans, Phys. Plasmas **11**, 3006 (2004).

[17] T. Onjun, A. H. Kritz, G. Bateman, V. Parail, H. Wilson, J. Lönnroth, G. Huysmans, and A. Dnestrovskij, Phys. Plasmas **11**, 1469 (2004).

[18] J.-S. Lönnroth, V. V. Parail, G. Corrigan *et al.*, Plasma Phys. Controlled Fusion **45**, 1689 (2003).

[19] T. Onjun, A. H. Kritz, G. Bateman, V. Parail, H. Wilson, and A. Dnestrovskij, Phys. Plasmas **12**, 012506 (2005).

[20] J.-S. Lönnroth, V. Parail, A. Dnestrovskij, C. Figarella, X. Garbet, H. Wilson and JET-EFDA contributors, Plasma Phys. Controlled Fusion **46**, 1197 (2004).

[21] H. R. Wilson, J. W. Connor, A. R. Field, S. J. Fielding, R. L. Miller, L. L. Lao, J. R. Ferron, and A. D. Turnbull, Phys. Plasmas **6**, 1925 (1999).

[22] P. Gohil, M. A. Mahdavi, L. Lao *et al.*, Phys. Rev. Lett. **61**, 1603 (1988).

[23] J. W. Connor, H. R. Hastie, H. R. Wilson, and R. L. Miller, Phys. Plasmas **5**, 2687 (1998).

[24] H. R. Wilson and R. L. Miller, Phys. Plasmas **6**, 873 (1999).

[25] J. Manickam, Phys. Fluids B **4**, 1901 (1992).

[26] M. Sugihara, Y. Igitkhanov, G. Janeschitz, A. E. Hubbard, Y. Kamada, J. Lingertat, T. H. Osborne, and W. Suttrop, Nucl. Fusion **40**, 1743 (2000).

[27] T. H. Osborne, K. H. Burrell, R. J. Groebner, L. L. Lao, A. W. Leonard, R. Maingi, R. L. Miller, G. D. Porter, G. M. Staebler, and A. D. Turnbull, J. Nucl. Mater. **266–269**, 131 (1999).

[28] D. Hannum, G. Bateman, J. Kinsey *et al.*, Phys. Plasmas **8**, 964 (2001).

[29] D. Boucher, J. Connor, W. Houlberg *et al.*, Nucl. Fusion **40**, 1955 (2000).

[30] T. H. Osborne, J. R. Ferron, R. J. Groebner *et al.*, Plasma Phys. Controlled Fusion **42**, A175 (2000).

[31] J. R. Ferron, M. S. Chu, G. L. Jackson *et al.*, Phys. Plasmas **7**, 1976 (2000).

[32] L. L. Lao, Y. Kamada, T. Oikawa *et al.*, Nucl. Fusion **41**, 295 (2001).

[33] H. Urano, Y. Kamada, H. Shirai *et al.*, Plasma Phys. Controlled Fusion **44**, 11 (2002).

[34] Y. Kamada, T. Hatae, T. Fukuda *et al.*, Plasma Phys. Controlled Fusion **41**, 1371 (1999).

[35] D. A. Mossessian, P. B. Snyder, M. Greenwald, J. W. Hughes, Y. Lin, A. Mazurenko, S. Medvedev, H. R. Wilson, and S. Wolfe, Plasma Phys. Controlled Fusion **44**, 423 (2002).

[36] Y. Kamada, K. Ushigusa, O. Naito *et al.*, Plasma Phys. Controlled Fusion **36**, A123 (1994).

[37] T. Hatae, Y. Kamada, S. Ishida *et al.*, Plasma Phys. Controlled Fusion **40**, 1073 (1998).

[38] Y. Koide and the JT–60U Team, Plasma Phys. Controlled Fusion **4**, 1623 (1997).

[39] The JET Team (presented by J. G. Cordey), in *Proceedings of the 17th International Atomic Energy Agency Fusion Energy Conference, Yokahama, Japan, 19–24 October 1998* (International Atomic Energy Agency, Vienna, 1999), Paper No. IAEA-F1-CN-69/EX7/1.

[40] J. Lingertat, V. Bhatnagar, G. D. Conway *et al.*, J. Nucl. Mater. **266–269**, 124 (1999).